UDC 62-50
DOI: 10.20535/SRIT.2308-8893.2023.3.07

IDENTIFICATION OF LUNG DISEASE TYPES USING CONVOLUTIONAL NEURAL NETWORK AND VGG-16 ARCHITECTURE

S. BUKHORI, B.Y.N. VERDY, Y.R. WINDI EKA, A.P. JANUAR

Abstract. Pneumonia, tuberculosis, and Covid-19 are different lung diseases but have similar characteristics. One of the reasons for the worsening of disease in lung sufferers is a diagnosis that takes a long time. Another factor, the results of the X-ray photos look blurry and lack contracture, causing different diagnostic results of X-ray photos. This research classifies lung images into four categories: normal lungs, tuberculosis, pneumonia, and Covid-19 using the Convolutional Neural Network method and VGG-16 architecture. The results of the research with models and scenarios without pre-trained use data with a ratio of 9:1 at epoch 50, anaccuracy of 94%, while the lowest results are in scenarios using data with a ratio of 8:2 at epoch 50, non-pre-trained models, accuracy by 87%.

Keywords: tuberculosis, pneumonia, Covid-19, VGG-16, convolutional neural network.

INTRODUCTION

Human internal organs that are often associated with external environmental factors, one of which is the lungs [1; 2]. The human lungs consist of two organs or a pair, namely the right and left. The lungs are located in the thoracic region of the human body, one of two large respiratory organs located in the chest cavityand are responsible for adding oxygen and removing carbon dioxide from the blood. The lungs have a rubbery texture and are pinkish-gray in colour. The lungs consist of other tissues inside which function to exchange oxygen and carbon dioxide [3]. Because of the process of exchanging oxygen and carbon dioxide, the lungs are in contact with external environmental factors such as smoke, microbes, dust and also chemicals in the environment as pollutants. The relationship with these environmental factors increases the risk of lung disease [4].

Several diseases can attack the lungs. Common symptoms are shortness of breath and coughing. Lung disorders can be acute or chronic. Several diseases that can attack the lungs and related respiratory systems include bronchitis, pneumonia, asthma, tuberculosis and Covid-19 [5]. Bronchitis is a respiratory disease that occurs as a result of an upper respiratory infection and is usually caused by a virus [6]. Pneumonia is a respiratory disorder that causes inflammation of the smallest parts of the lungs, namely the bronchioles and alveolar tissue. Asthma is a disease caused by inflammation of the respiratory tract. This inflammation will cause swelling and narrowing of the airways. Air that should flow into the lungs becomes obstructed [7]. Tuberculosis is a bacterial infection caused by Mycobacterium tuberculosis which attacks and damages body tissues. Bacteria can be transmitted through the airways. Tuberculosis generally attacks the lungs, but also

has the risk of spreading to the lymph nodes, bones, central nervous system, heart and other organs [8]. Covid-19 is an infectious disease caused by SARS-CoV-2, a type of coronavirus [9]. Typical symptoms are fever, cough, flu and shortness of breath. Covid-19 spreads from one person to another through droplets from the respiratory tract which are often produced when coughing or sneezing. Droplet range is usually up to 1 meter [10]. Droplets can stick to objects, but won't last long in the air. The time from transmission of the virus to the onset of clinical symptoms is between 1–14 days with an average of 5 days. Bronchitis, pneumonia, asthma, tuberculosis and Covid-19 if not handled properly in a short time can cause health complications [11].

Lung disease problems tend to increase due to delays in diagnosis. Diagnosis takes a long time because of the similarities in the symptoms of lung disease. According to WHO, various lung diseases including pneumonia, tuberculosis and Covid-19 have almost the same symptoms [12]. One of the main reasons for the increase in lung disease problems during the Covid-19 pandemic is the long process of diagnosis. Another factor is that X-Rays often appear blurry and have no contractures, leading to a different diagnosis [13]. Additional laboratory test results are needed to identify whether it is classified as tuberculosis, pneumonia, or Covid-19. One of the reasons for the unfavourable radiographic results is the difference in X-Ray intensity in photos of normal tissue and photos of glandular tissue affected by lung disease [14]. To overcome this problem, image processing is needed so that it can increase and improve image quality. A lung disease classification system is needed to help diagnose lung disease quickly. Alternative technologies that can be used to overcome this problem are the use of computer vision and deep learning.

Computer vision is one part of artificial intelligence [15]. Computer Vision is a technology that allows computers to recognize objects around them [16]. Science and technology are developing very fast, especially in the development of computer vision combined with deep learning. Deep learning can be used for decision making, detecting diseases based on their symptoms and early detection [17]. This research develops identification of lung disease types using Convolutional Neural Network and VGG-16 architecture.

Several research have identified lung disease from chest X-Rays using small volume datasets and applying machine learning [15; 18]. The results of applying this technology are quite important for medical progress. Research related to the early diagnosis and treatment of lung diseases using deep learning has also been researched and the results are quite important in clinical treatment [19; 20; 21]. This research develops lung disease identification using Convolutional Neural Network (CNN) and VGG-16 architecture. CNN with VGG-16 architecture has higher accuracy than other network architectures in processing ImageNet datasets [22]. In similar cases, classification of pneumonia from X-Ray images using VGG-16 results 97.93 % accuracy, while classification of pneumonia from X-Ray images using inception-V3 results 96.58% accuracy [23]. The inception-V3 is the latest version developed from the inception-V1 and V2 models. The inception-V3 model is a CNN trained directly on a low-configuration computer. The training is quite difficult, and takes much longer. This problem is solved through transfer learning which saves the last layer of the model for the new category. The parameters of the previous layer are stored, and the inception-V3 model is deconstructed when the last layer is removed using transfer learning techniques. CNNs inception is a network in the form of a repeated convolution design configuration

pattern. The components in CNNs inception are input layer, 1×1 convolution layer, 3×3 convolution layer, 5×5 convolution layer, max pooling layer, and concatenation layer [24].

Test results on the diagnosis of pneumonia showed that VGG-16 architecture exceed Xception network at the accuracy with 87% and 82% respectively [25]. Xception is a development of inception. The inception model was developed with depth wise separable convolution. The number of parameters is almost the same as inception. Xception brings the inception hypothesis to eXtreme. First, the cross-feature map is captured by a 1×1 convolution. Consequently, the correlation of each channel is captured via a regular 3×3 or 5×5 convolution. This idea goes to the extreme of doing 1×1 to each channel, then doing 3×3 to each output [26]. This is identical to replacing the inception module with depth wise separable convolutions. With a higher level of accuracy, the VGG-16 architecture can increase the value of lung disease classification based on CT-scan images. This research also developed a classification of lung images into four classes, namely normal lungs, tuberculosis, pneumonia, and Covid-19.

The rest of this paper is organized as follows: The proposed model for identification of lung disease types using CNN and VGG-16 architecture is discussed in section 2. Section 3 provides a system design for identification of lung disease types using CNN and VGG-16 architecture. Section 4 discusses the results and analysis of CNN model and integrated system applications. Finally, conclusions are given in section 5.

RESEARCH PROPOSED

CNN architecture developed using VGG-16. The proposed architecture has 13 convolution layers and 3 fully connected layers so that a total of 16 layers are used, there are 5 max-polling layers which are forwarded to several convolution layers. Each layer has a different image size, on the first layer the image will be resized to 224×224, then on the next layer the image size will be reduced to 112×112, 56×56, 28×28, 14×14 as shown in Fig. 1.

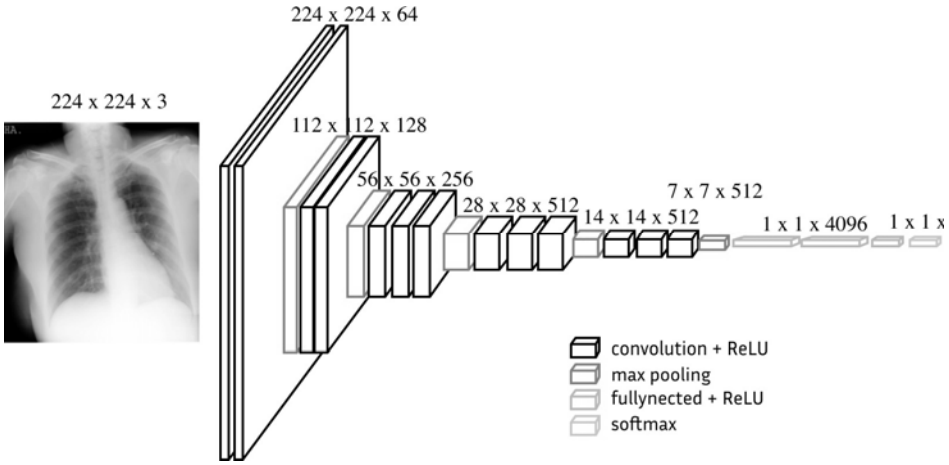

Fig. 1. The Proposed Model

Fig. 1 shows that the first layer is a fully connected layer which has 4096 neurons, the second layer has 4096 neurons, and the third layer has 4 neurons. In

the last layer there are 4 layers according to the number of classifications, namely normal, pneumonia, tuberculosis, and Covid-19. There are several layers in the CNN architecture (Fig. 1) which are used in the training and testing process. This architecture is designed to produce models with better accuracy.

Input image is the process of entering an input file in the form of a chest X-Ray image. Before the data is entered into the training process, to prevent errors in classification, the dataset is adjusted specifically for biased data or truncated data. Inappropriate data will be discarded and appropriate data will be included in a dataset that is ready to be classified. This process includes 3 stages, namely changing the size of the photo with a target of 224×224 pixels, the photo data is separated into two parts, namely training data and testing data with a comparison ratio of 7 : 3, 8 : 2, and 9 : 1. Then the photo is converted from RGB to grayscale.

The convolutional layer includes filter, kernel, stride, Relu activation, and poolingoperations. The convolution layer used in this research uses a kernel with a size of 3×3 pixels and the number of strides is 1, and uses a padding configuration. There are thirteen convolution layers, the first convolution layer uses 64 filters,the kernel is 3×3 pixels. The size of the chest X-Ray is 224×224 pixels which then uses the ReLu activation function. The second convolution layer is similar to the first convolution process but continues with a pooling operation with a strides size of 2×2 and a pooling size of 2×2. The pooling operation will produce an image measuring 112×112 pixels and a total of 64 feature maps. This feature map will be included into the third convolution process. The third convlution layer has different parameters from the previous layer. The filter used in the third layer is 128 with a data input size of 112×112 pixels. With a total of 128 filters, the third convolution feature map obtained is 128. The fourth convolution layer is similar to the third convolution process, but the pooling operation is continued with a strides size of 2×2 and a pooling size of 2×2. The pooling operation will produce an image measuring 56 × 56 pixels and a total of 128 feature maps. This feature map will be included in the in the fifth convolution process. The fifth convolution layer has different parameters from the fourth layer. There are 256 filters used in this fifth layer with an input data size of 56 × 56 pixels. With a total of 256 filters, the convolution of the five feature maps obtained is 256. The sixth convolution layer is similar to the fifth convolution layer without changing any parameters. The filters used in the sixth layer are 256 with a data input size of 56 × 56 pixels. The seventh convolution layer has similarities with the fifth and sixth convolution layers without changing any parameters. The filters used in the seventh layer are 256 with a data input size of 56×56 pixels. In this layer, pooling operations are continued with a strides size of 2×2 and a pooling size of 2×2. The pooling operation will produce an image measuring 28×28 pixels anda total of 256 feature maps. The eighth convolution layer has different parameters from the previous layer. The filter used in this eighth layer is 512 with a data input size of 28×28 pixels. Because there are 512 filters, the eighth convolution produces 512 feature maps. The ninth convolution layer has the same parameters as the eighth convolution layer. The filter used in the ninth layer is 512 and the input data is 28×28 pixels. Filters with a total of 512 in the ninth convolution produce a feature map totaling 512. The tenth convolution layer has the same parameters as the eighth and ninth convolution layers. The filter used in the tenth layer is 512 and the input data is 28×28 pixels. This process is followed by a pooling operation with strides size of 2×2 and a pooling size of 2×2. Thepooling operation will produce an

image size of 14×14 pixels and a total of 512 feature maps. The eleventh convolution layer has similarities with the tenth layer, but has a different input data size. The filter used in the eleventh layer is 512 with a data input size of 14×14 pixels. There are 512 filters and in the eleventh convolution, the resulting feature maps are 512. The twelfth convolution layer has the same parameters as the eleventh convolution layer. The filter used is 512 with a data input size of 14×14 pixels. These 512 filters will produce a feature map of 512. The thirteenth convolution layer has the same parameters as the eleventh and twelfth layers. The filter used is 512 with input data of 14×14 pixels. Then the process is continued with a pooling operation with a size of 2×2 strides and a pooling size of 2×2. The pooling operation will produce an image measuring c pixels and a total of 512 feature maps.

The flatten layer is the layer that converts the multidimensional array output in the feature extraction process into a one-dimensional matrix which is then followed by the fully connected layer process. While the fully connected layer will be used as many as three fully connected layers. The first layer is 4096, the second layer is 4096, and the last layer is 4 according to the classification designed.

SYSTEM DESIGN

The system is designed using the CNN architecture with 16 layers according to the VGG-16 architectural concept. The architectural design uses 13 convolution layers and 3 fully connected layers so that the total layers used are 16 layers. This research uses 5 layers of max-polling, which adjusts to several convolution layers. Each layer has a different image size. The first layer will resize the image to 224×224, then the next layer will reduce the size of the image to a configuration of 112×112, 56×56, 28×28, 14×14, and 7×7, as shown in Table 1.

Table 1. Configuration VGG-16

No.	Layer	Output Shape
1	Conv2D	224, 224, 64
2	Conv2D	224, 224, 64
3	MaxPooling2D	112, 112, 64
4	Conv2D	112, 112, 128
5	Conv2D	112, 112, 128
6	MaxPooling2D	56, 56, 128
7	Conv2D	56, 56, 256
8	Conv2D	56, 56, 256
9	Conv2D	56, 56, 256
10	MaxPooling2D	28, 28, 256
11	Conv2D	28, 28, 512
12	Conv2D	28, 28, 512
13	Conv2D	28, 28, 512
14	MaxPooling2D	14, 14, 512
15	Conv2D	14, 14, 512
16	Conv2D	14, 14, 512
17	Conv2D	14, 14, 512
18	MaxPooling2D	7, 7, 512
19	Flatten	25088
20	Dense	4096
21	Dense	4096
22	Dense	4

After modeling, it is continued with testing of the CNN model that has been designed to analyze the accuracy of the model by changing the data scenario, epoch and using pre-trained models. This process aims to select a model that has the highest accuracy so that it can be used for classification. Before comparing accuracy, the model will conduct data training and data testing with a ratio of 7 : 3, 8 : 2 and 9 : 1.

The test was carried out by changing the parameters to get the best image results for the classification of normal lungs, lungs with tuberculosis, lungs with pneumonia, and lungs with Covid-19. This research was conducted using three different epochs, namely: epoch 20, epoch 50, and

epoch 100.While the data scenario uses three different data scenarios from each epoch that are used, namely scenario data 7 : 3, 8: 2 and 9: 1, and uses a comparison between using the pre- training and without using the pre-training model. Then the model will be compared for its level of accuracy and will be selected through the model with thehighest accuracy.

RESULTS AND ANALYSIS

The model that has been designed is tested to get the best scenario. Scenarios are made based on the number of epochs and the amount of data. The number of epochs tested were 20, 50, and 100, while the amount of data used was a ratio of 7 : 3, 8 : 2, and 9 : 1. Model testing was also carried out on models with pre-training and models without training.

Each scenario has a different value when using a different number of epochs, even though the model used is the same. Comparison of the performance of the CNN model as a whole and the test results are shown in Table 2 – Table 4 for the non-pretrained model test cases; Table 5 – Table 7 for the test cases with the pretrained model.

Table 2. Performance comparison with data ratio of 7 : 3 (non-pretrained)

Performance	***Epoch***		
	20	50	100
Data Scenario 7 : 3			
Accuracy	87.33%	89%	90%
Precision	89%	90%	90%
Recall	87%	89%	90%
F1 score	87%	89%	90%
Learning Curve	overfitting	overfitting	overfitting

The best performance on scenario data with a ratio of 7 : 3 (non–pretrained) is at epoch 100 with an accuracy value of 90%, a precision value of 90%, a recall valueof 90%, and a F1 score value of 90%. The results of the learning curves in this scenario have a high variance as shown in Fig. 2. The occurrence of a high variance indicates that there has been overfitting.

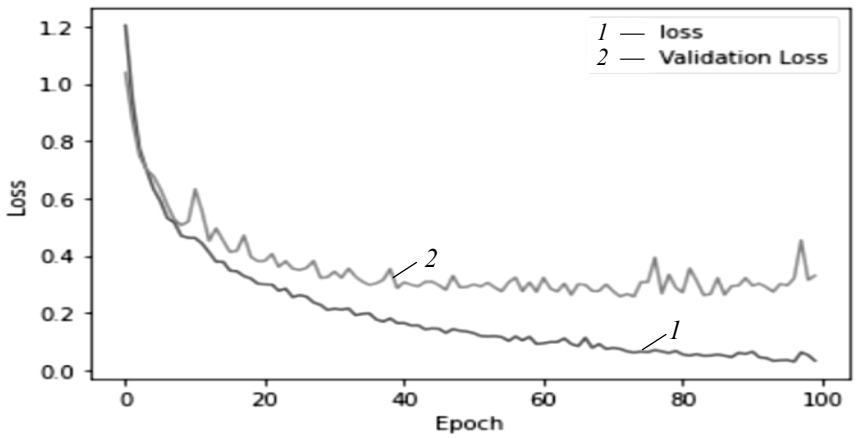

Fig. 2. Learning Curve Data Scenario 7 : 3 Epoch 100

Table 3. Performance comparison with data ratio of 8 : 2 (non-pretrained)

Performance	***Epoch***		
	20	50	100
Data Scenario 8 : 2			
Accuracy	87%	90.25%	92%
Precision	88%	90%	92%
Recall	87%	90%	92%
F1 score	87%	90%	92%
Learning Curve	overfitting	overfitting	overfitting

The best performance on scenario data with a ratio of 8 : 2 (non-pretrained) is at epoch 100 with an accuracy value of 92%, a precision value of 92%, a recall valueof 92%, and a F1 score value of 92%. The results of the learning curves in this scenario have a high variance as shown in Fig. 3. The occurrence of a high variance indicates that there has been overfitting.

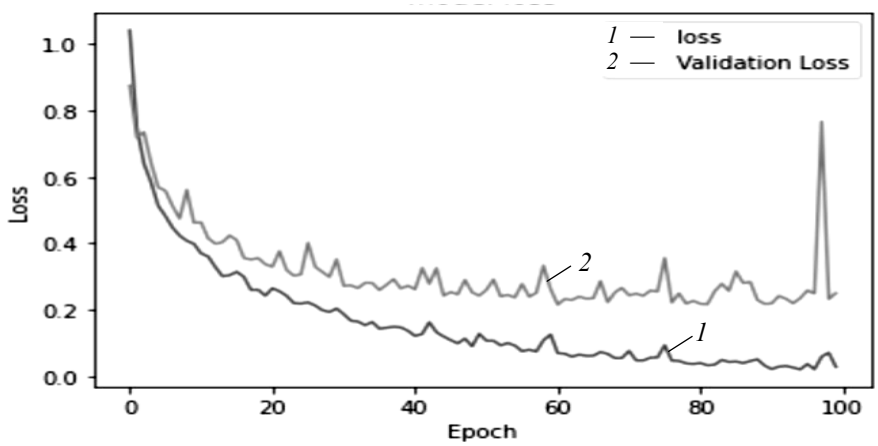

Fig. 3. Learning Curve Data Scenario 8 : 2 Epoch 100

Table 4. Performance comparison with data ratio of 9 : 1 (non-pretrained)

Performance	***Epoch***		
	20	50	100
Data Scenario 9 : 1			
Accuracy	89.50%	94%	92%
Precision	89%	94%	91%
Recall	89%	94%	93%
F1 score	90%	94%	92%
Learning Curve	overfitting	overfitting	overfitting

The best performance on scenario data with a ratio of 9 : 1 (non-pretrained) is at epoch 50 with an accuracy value of 94%, a precision value of 94%, a recall value of 94%, and a F1 score value of 94%. The results of the learning curves in this scenario have a high variance as shown in Fig. 4. The occurrence of a high variance indicates that there has been overfitting.

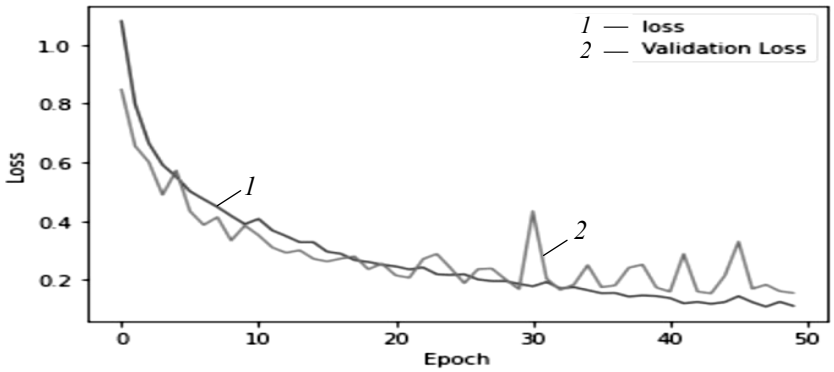

Fig. 4. Learning Curve Data Scenario 9 : 1 Epoch 50

T a b l e 5. Performance comparison with data ratio of 7 : 3 (pretrained)

Performance	***Epoch***		
	20	50	100
Data Scenario 7 : 3			
Accuracy	91%	91.17%	91.33%
Precision	91%	92%	92%
Recall	91%	91%	91%
F1 score	91%	91%	91%
Learning Curve	overfitting	overfitting	overfitting

The best performance on scenario data with a ratio of 7 : 3 (pretrained) is at epoch 100 with an accuracy value of 91.33%, a precision value of 92%, a recall value of 91%, and a F1 score value of 91%. The results of the learning curves in this scenario have a high variance as shown in Fig. 5. The occurrence of a high variance indicates that there has been overfitting.

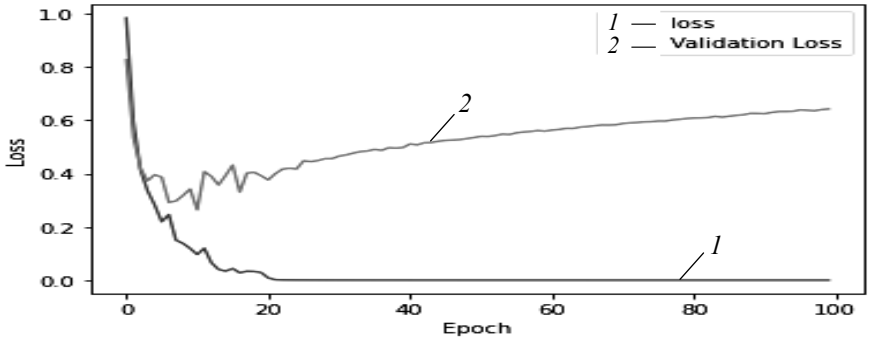

Fig. 5. Learning Curve Data Scenario 7 : 3 Epoch 100

T a b l e 6. Performance comparison with data ratio of 8 : 2 (pretrained)

Performance	***Epoch***		
	20	50	100
Data Scenario 8 : 2			
Accuracy	91%	93.75%	92.50%
Precision	92%	94%	92%
Recall	91%	94%	92%
F1 score	91%	94%	93%
Learning Curve	overfitting	overfitting	overfitting

The best performance on scenario data with a ratio of 8 : 2 (pretrained) is at epoch 50 with an accuracy value of 93.75%, a precision value of 94%, a recall value of 94%, and a F1 score value of 94%. The results of the learning curves in this scenario have a high variance as shown in Fig. 6. The occurrence of a high variance indicates that there has been overfitting.

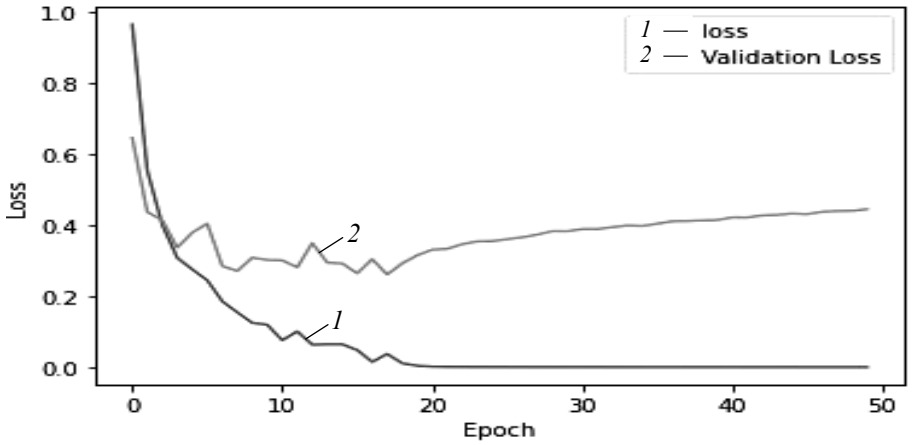

Fig. 6. Learning Curve Data Scenario 8 : 2 Epoch 50

T a b l e 7. Performance comparison with data ratio of 9 : 1 (pretrained)

Performance	***Epoch***		
	20	50	100
Data Scenario 9 : 1			
Accuracy	94%	95%	94.50%
Precision	94%	96%	93%
Recall	94%	95%	94%
F1 score	94%	95%	94%
Learning Curve	overfitting	overfitting	overfitting

The best performance on scenario data with a ratio of 9 : 1 (pretrained) is at epoch 50 with an accuracy value of 95%, a precision value of 96%, a recall value of 95%, and a F1 score value of 95%. The results of the learning curves in this scenario have a high variance as shown in Fig. 7. The occurrence of a high variance indicates that there has been overfitting.

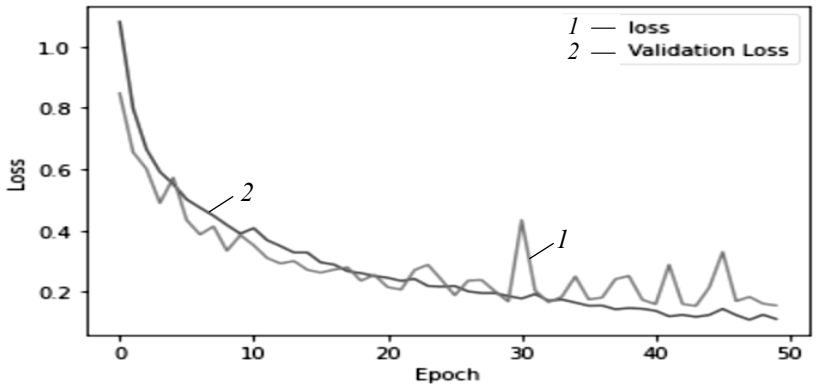

Fig. 7. Learning Curve Data Scenario 9 : 1 Epoch 50

CONCLUSIONS

Convolutional Neural Network classification model is tested by training the model using training data and testing the accuracy of the model with testing data. The better the model, the better the accuracy obtained. Testing results show that the CNN model has the highest accuracy in the scenario of non-pretrained data model 9 : 1 at epoch 50 which is 94%, while the lowest result is at 8 : 2 epoch 50 scenario testing of data without using a pre-trained model with an accuracy of 87%.

The model from this scenario will be used to be implemented into applications because it has the best accuracy among models with other scenarios. The pulmonary infectious disease classification system classifies pulmonary infectious diseases based on chest X-Rays uploaded by doctors/health workers with good accuracy. This system can classify into four classes: Normal, Covid-19, Pneumonia, and Tuberculosis. Pretraining models, epochs, and data scenarios can impact model performance. This research has conducted tests to determine the best performance achieved by using the VGG-16 architecture. The best performance is obtained in the 9 : 1 data scenario, epoch 50 on the non pre-trainedmodel, with an accuracy value of 94%, precision value of 94%, recall value of 94%, and F1-score value of 94%, while the lowest result is in the 8 : 2 data scenario test epoch 50 on the non-pretrained model with an accuracy value of 87%, precision value of 88%, recall value of 87%, and F1-score value of 87%.

REFERENCES

1. K.F. Budden et al., “Emerging pathogenic links between microbiota and the gut-lung axis,” *Nat. Rev. Microbiol.*, vol. 15, no. 1, pp. 55–63, 2017. doi: 10.1038/nrmicro.2016.142.
2. P.K. Wang L., F.H. Green, and S.M. Smiley-Jewell, “乳鼠心肌提取 HHS Public Access,”*Susceptibility aging lung to Environ. Inj.*, vol. 176, no. 1, pp. 539–553, 2010. doi: 10.1055/s-0030-1265895.
3. D.J. Randall, “Transport and exchange of respiratory gases in the blood | Carbon Dioxide Transport and Excretion,” *Encycl. Fish Physiol.*, vol. 2, pp. 909–915, Dec. 2011. doi: 10.1016/B978-0-12-374553-8.00027-7.
4. F. Yu, R. Xiao, X. Li, Z. Hu, L. Cai, and F. He, “Combined effects of lung disease history, environmental exposures, and family history of lung cancer to susceptibility of lung cancer in Chinese non-smokers,” *Respir. Res.*, vol. 22, no. 1, pp. 1–10, 2021. doi: 10.1186/s12931-021-01802-z.
5. N. Clementi et al., “Viral respiratory pathogens and lung injury,” *Clin. Microbiol. Rev.*, vol. 34, no. 3, pp. 1–45, 2021. doi: 10.1128/CMR.00103-20.
6. U. Grote, A. Fasse, T.T. Nguyen, and O. Erenstein, “Food Security and the Dynamics of Wheat and Maize Value Chains in Africa and Asia,” *Front. Sustain. Food Syst.*, vol. 4, no. February, pp. 1–17, 2021. doi: 10.3389/fsufs.2020.617009.
7. L.J. Quinton, A.J. Walkey, and J.P. Mizgerd, “Integrative physiology of pneumonia,” *Physiol. Rev.*, vol. 98, no. 3, pp. 1417–1464, 2018. doi: 10.1152/PHYSREV.00032.2017.
8. R. Gopalaswamy, S. Shanmugam, R. Mondal, and S. Subbian, “Of tuberculosis and non-tuberculous mycobacterial infections - A comparative analysis of epidemiology, diagnosis and treatment,” *J. Biomed. Sci.*, vol. 27, no. 1, pp. 1–17, 2020. doi: 10.1186/s12929-020-00667-6.
9. M.T. Adil et al., “SARS-CoV-2 and the pandemic of COVID-19,” *Postgrad. Med. J.*, vol. 97, no. 1144, pp. 110–116, 2021. doi: 10.1136/postgradmedj-2020-138386.

10. L. Morawska and J. Cao, “Airborne transmission of SARS-CoV-2: The world should face the reality,” *Environ. Int.*, vol. 139, no. April, p. 105730, 2020. doi: 10.1016/j.envint.2020.105730.
11. M. Wei, Y. Zhao, Z. Qian, B. Yang, J. Xi, and J. Wei, “Pneumonia caused by Mycobacterium tuberculosis,” *Microbes Infect.*, no. January, 2020.
12. “Clinical management of severe acute respiratory infection (SARI) when COVID-19 disease is suspected,” *World Health Organization*, 2020. [Online]. Available: https://www.ptonline.com/articles/how-to-get-better-mfi-results
13. R. Yasin and W. Gouda, “Chest X-ray findings monitoring COVID-19 disease course and severity,” *Egypt. J. Radiol. Nucl. Med.*, vol. 51, no. 1, 2020. doi: 10.1186/s43055-020-00296-x.
14. A.M. O’Hare et al., “Complexity and Challenges of the Clinical Diagnosis and Management of Long COVID,” *JAMA Netw. Open*, vol. 5, no. 11, p. e2240332, 2022. doi: 10.1001/jamanetworkopen.2022.40332.
15. A.I. Khan and S. Al-Habsi, “Machine Learning in Computer Vision,” *Procedia Comput. Sci.*, vol. 167, no. 2019, pp. 1444–1451, 2020. doi: 10.1016/j.procs.2020.03.355.
16. S. Wael, A. Elshater, and S. Afifi, “Mapping User Experiences around Transit Stops Using Computer Vision Technology: Action Priorities from Cairo,” *Sustain.*, vol. 14, no. 17, 2022. doi: 10.3390/su141711008.
17. S. Arooj, S.U. Rehman, A. Imran, A. Almuhaimeed, A.K. Alzahrani, and A. Alzahrani, “A Deep Convolutional Neural Network for the Early Detection of Heart Disease,” *Biomedicines*, vol. 10, no. 11, p. 2796, 2022. doi: 10.3390/biomedicines10112796.
18. Y. Erdaw and E. Tachbele, “Machine learning model applied on chest X-ray images enables automatic detection of COVID-19 cases with high accuracy,” *Int. J. Gen. Med.*, vol. 14, pp. 4923–4931, 2021, doi: 10.2147/IJGM.S325609.
19. T.N. Sree Ganesh, R. Satish, and R. Sridhar, “Learning effective embedding for automated COVID-19 prediction from chest X-ray images,” *Multimed. Syst.*, no. 0123456789, 2022. doi: 10.1007/s00530-022-01015-4.
20. S.M. Fati, E.M. Senan, and N. ElHakim, “Deep and Hybrid Learning Technique for Early Detection of Tuberculosis Based on X-ray Images Using Feature Fusion,” *Appl. Sci.*, vol. 12, no. 14, 2022. doi: 10.3390/app12147092.
21. V. Acharya et al., “AI-Assisted Tuberculosis Detection and Classification from Chest X-Rays Using a Deep Learning Normalization-Free Network Model,” *Comput. Intell. Neurosci.*, vol. 2022, p. 2399428, 2022. doi: 10.1155/2022/2399428.
22. H. Handoko, F. Rozy, F.E. Gani, and A. Dharma, “Comparative Analysis of Convolutional Neural Network Methods in Detecting Mask Wear,” *Budapest International Research and Critics Institute-Journal (BIRCI-Journal*), 5(2), 2022.
23. M. Mujahid, F. Rustam, R. Álvarez, J. Luis Vidal Mazón, I. de la T. Díez, and I. Ashraf, “Pneumonia Classification from X-ray Images with Inception-V3 and Convolutional Neural Network,” *Diagnostics*, vol. 12, no. 5, pp. 1–16, 2022. doi: 10.3390/diagnostics12051280.
24. G. Natarajan and P. Dhanalakshmi, “Classification of pneumonia using pre-trained convolutional networks on chest X-Ray images,” *Int. J. Health Sci. (Qassim)*, vol. 6, no. April, pp. 5378–5390, 2022. doi: 10.53730/ijhs.v6ns1.6097.
25. E. Ayan and H.M. Ünver, “Diagnosis of pneumonia from chest X-ray images using deep learning,” *2019 Sci. Meet. Electr. Biomed. Eng. Comput. Sci. EBBT 2019*, pp. 10–13, 2019. doi: 10.1109/EBBT.2019.8741582.
26. Y.-J. Fan et al., “Machine Learning: Using Xception, a Deep Convolutional Neural Network Architecture, to Implement Pectus Excavatum Diagnostic Tool from Frontal-View Chest X-rays,” *Biomedicines*, vol. 11, no. 3, p. 760, 2023. doi: 10.3390/biomedicines11030760.

Received 05.01.2023

INFORMATION ON THE ARTICLE

Saiful Bukhori, ORCID: 0000-0002-2527-1080, University of Jember, Indonesia, e-mail: saiful.ilkom@unej.ac.id

Verdy Bangkit Yudho Negoro, University of Jember, Indonesia, e-mail: verdybangkit@gmail.com

Windi Eka Yulia Retnani, ORCID: 0009-0001-7838-0205, University of Jember, Indonesia, e-mail: windi.ilkom@unej.ac.id

Januar Adi Putra, University of Jember, Indonesia, e-mail: januaradi.putra@unej.ac.id

ІДЕНТИФІКАЦІЯ ТИПІВ ЗАХВОРЮВАННЯ ЛЕГЕНЬ ЗА ДОПОМОГОЮ ЗГОРТКОВОЇ НЕЙРОННОЇ МЕРЕЖІ Й АРХІТЕКТУРИ VGG-16 / Сайфул Бухорі, Верді Бангкіт Юдхо Негоро, Вінді Ека Юліа Ретнані, Януар Аді Путра

Анотація. Пневмонія, туберкульоз і Covid-19 – різні захворювання легенів, але мають схожі характеристики. Однією з причин загострення захворювання легень є довготривала діагностика. Іншим фактором є те, що результати рентгенівських знімків виглядають розмитими і з відсутністю контрактури, що спричиняє різні результати діагностики рентгенівських знімків. Це дослідження класифікує зображення легенів на чотири категорії, а саме: нормальні легені, туберкульоз, пневмонія та Covid-19 за допомогою методу згорткової нейронної мережі та архітектури VGG-16. Результати дослідження з моделями та сценаріями без попередньої підготовки використовують дані зі співвідношенням 9:1 в епосі 50, точністю 94%, тоді як найнижчі результати в сценаріях з використанням даних зі співвідношенням 8:2 в епосі 50, моделі без попередньої підготовки, точність 87%.

Ключові слова: туберкульоз, пневмонія, Covid-19, VGG-16, згорткова нейронна мережа.